

# A note on dimer models and McKay quivers

Kazushi Ueda and Masahito Yamazaki

## Abstract

We give one formulation of an algorithm of Hanany and Vegh [15] which takes a lattice polygon as an input and produces a set of isoradial dimer models. We study the case of lattice triangles in detail and discuss the relation with coamoebas following Feng, He, Kennaway and Vafa [7].

## 1 Introduction

Dimer models are introduced in 1930s as a statistical mechanical model for adsorption of di-atomic molecules on the surface of a crystal [8]. A dimer model in this sense is a graph consisting of the set  $N$  of nodes and the set  $E$  of edges, together with a function  $\mathcal{E} : E \rightarrow \mathbb{R}$  which represents the energy of adsorption. A *perfect matching* is a subset  $D$  of  $E$  such that for any node  $n \in N$ , there exists a unique edge  $e \in D$  adjacent to  $n$ , and one is interested in the asymptotic behavior of the partition function

$$Z = \sum_{D : \text{a perfect matching}} \exp \left( -\beta \sum_{e \in D} \mathcal{E}(e) \right)$$

as the graph becomes large. Many interesting statistical mechanical models such as domino tilings, Ising models and plane partitions can be realized as a dimer model on a particular planar graph. See e.g. [20] for a review on dimer models.

In 1961, Kasteleyn [18] introduced a method to represent the partition function as the determinant of a weighted adjacency matrix, called the Kasteleyn matrix. This is used to great effect by Kenyon, Okounkov and Sheffield [21] to study dimer models on periodic bipartite graph. The determinant of the Kasteleyn matrix with respect to a particular weighting is called the *characteristic polynomial*, and plays an essential role in their work. It is a Laurent polynomial in two variables whose Newton polygon, called the *characteristic polygon*, contains the information of possible asymptotic behavior of the periodic dimer model on the universal cover of the torus.

Recent advances in string theory have uncovered a new connection between dimer models and geometry, culminating in the proposal that a bicolored isoradial graph on a torus produces an AdS/CFT dual pair of a toric Sasaki-Einstein 5-manifold and an  $N = 1$  superconformal field theory in four dimensions [9, 10, 14]. Isoradiality is needed for the existence of *R-charges* in superconformal field theory, which is dual to volumes of Sasaki-Einstein manifolds [1, 3, 4, 19, 23, 24, 25].

The toric Calabi-Yau 3-fold, obtained as the metric cone over the Sasaki-Einstein 5-manifold, is determined by the characteristic polygon. The dual superconformal field

theory is determined by a quiver with potential, which is obtained as the dual graph of the bicolored graph. Isoradiality implies [27, 2, 5, 16] that the path algebra of this quiver with potential is a Calabi-Yau algebra in the sense of Ginzburg [12], and the toric Calabi-Yau 3-fold can be obtained as the moduli space of representations of the quiver [11, 17].

An inverse construction of a bicolored isoradial graph on a torus from a convex lattice polygon is studied by Hanany and Vegh [15]. Following their work, we formulate the *linear Hanany-Vegh algorithm*, which takes a convex lattice polygon as an input and produces a set of bicolored graphs on a torus. The adjective *linear* comes from the fact that *zig-zag paths* in the resulting graph behave like lines, which enables one to show the following:

**Theorem 1.1.** *Let  $\Delta$  be a convex lattice polygon and  $G$  be a bicolored graph obtained from  $\Delta$  by the linear Hanany-Vegh algorithm. Then  $G$  is isoradial and  $\Delta$  coincides with the characteristic polygon of  $G$  up to translation.*

Although it is difficult to enumerate the output of the linear Hanany-Vegh algorithm in general, one can give a complete description when the input is a triangle:

**Theorem 1.2.** *If the input of the linear Hanany-Vegh algorithm is a lattice triangle, then the output consists of a unique graph which is dual to the McKay quiver.*

See [33] for another attempt to give a mathematical formulation of the algorithm of Hanany and Vegh, and [13, 16, 32] for an alternative algorithm due to Gulotta.

An important aspect of dimer models is their relation with mirror symmetry. The mirror of the toric Calabi-Yau 3-fold is an algebraic curve in  $(\mathbb{C}^\times)^2$ , which governs the *limit shape* of the melting crystal model associated with the bicolored graph [29, 30]. The *coamoeba* of this curve is defined by Passare and Tsikh as its image by the argument map

$$\begin{array}{ccc} \text{Arg} : (\mathbb{C}^\times)^2 & \rightarrow & (\mathbb{R}/\mathbb{Z})^2 \\ \Psi & & \Psi \\ (x, y) & \mapsto & \frac{1}{2\pi} (\arg(x), \arg(y)), \end{array} \quad (1.1)$$

whose behavior is expected by Feng, He, Kennaway and Vafa [7] to be described by the bicolored graph.

We show the following in this paper:

**Theorem 1.3.** *Let  $\Delta$  be a lattice triangle and  $W$  be the Laurent polynomial obtained as the sum of monomials corresponding to the vertices of  $\Delta$ . Then the bicolored graph obtained in Theorem 1.2 is a deformation retract of the coamoeba.*

A more detailed description of the coamoeba in this case in terms of the McKay quiver of an abelian subgroup of  $SL_3(\mathbb{C})$  is given in Theorem 7.1. The proof is based on the identification of the torus  $(\mathbb{C}^\times)^2$  with the dual of a maximal torus of  $SL_3(\mathbb{C})$ . This point of view will be used in [34] to study equivariant homological mirror symmetry for two-dimensional toric Fano stacks.

The organization of this paper is as follows: In Section 2, we recall basic definitions on dimer models. In Section 3, we formulate the linear Hanany-Vegh algorithm. Theorem 1.1 is proved in Section 4. In Section 5, we recall the identification of McKay quivers with hexagonal tilings of a real 2-torus and prove Theorem 1.2. We discuss the asymptotic behavior of coamoebas in Section 6, and study the case of the sum of three monomials in detail in Section 7.

## 2 Characteristic polygon of a dimer model

Let  $N = \mathbb{Z}^2$  be a free abelian group of rank two and  $M = \text{Hom}(N, \mathbb{Z})$  be the dual group. Put  $M_{\mathbb{R}} = M \otimes \mathbb{R}$  and  $T^{\vee} = M_{\mathbb{R}}/M$ . We fix the standard orientation and the Euclidean inner product on  $M_{\mathbb{R}} \cong \mathbb{R}^2$ .

- A *graph* on  $T^{\vee}$  consists of
  - a finite subset  $N \subset T^{\vee}$  called the set of *nodes*, and
  - another finite set  $E$  called the set of *edges*, consisting of continuous maps  $e : [0, 1] \rightarrow T^{\vee}$ ,

such that

$$e(0) \in N, \quad e(1) \in N, \quad e((0, 1)) \cap N = \emptyset,$$

and

$$e((0, 1)) \cap e'((0, 1)) = \emptyset$$

for not necessarily distinct edges  $e, e' \in E$ .

- A pair  $(n, e)$  of a node and an edge of a graph is said to be *adjacent* if  $e(0) = n$  or  $e(1) = n$ .
- A graph is said to be *bipartite* if the set of nodes can be divided into two disjoint set  $N = B \sqcup W$  so that every edge is adjacent both to an element of  $B$  and  $W$ .
- A *bicolored graph* is a bipartite graph together with a choice of a division  $N = B \sqcup W$  satisfying the condition above. The elements of  $B$  and  $W$  are said to be *black* and *white* respectively.
- A *face* of a graph on  $T^{\vee}$  is a connected component of the complement of the set of (the images of) edges.
- A bicolored graph on  $T^{\vee}$  is a *dimer model* if every face is simply-connected.
- A *perfect matching* on a dimer model  $G = (B, W, E)$  is a subset  $D \subset E$  such that for every node  $n \in B \cup W$ , there is a unique edge  $e \in D$  adjacent to it.

Let  $G$  be a dimer model and consider the bicolored graph  $\tilde{G}$  on  $M_{\mathbb{R}}$  obtained from  $G$  by pulling-back by the natural projection  $M_{\mathbb{R}} \rightarrow T^{\vee}$ . The set of perfect matchings of  $G$  can naturally be identified with the set of periodic perfect matchings of  $\tilde{G}$ . Fix a reference perfect matching  $D_0$ . Then for any perfect matching  $D$ , the union  $D \cup D_0$  divides  $M_{\mathbb{R}}$  into connected components. The height function  $h_{D, D_0}$  is a locally-constant function on  $M_{\mathbb{R}} \setminus (D \cup D_0)$  which increases (resp. decreases) by 1 when one crosses an edge  $e \in D$  with the black (resp. white) vertex on the right or an edge  $e \in D_0$  with the white (resp. black) vertex on the right. This rule determines the height function up to an additive constant. The height function may not be periodic even if  $D$  and  $D_0$  are periodic, and the *height change*  $h(D, D_0) = (h_x(D, D_0), h_y(D, D_0)) \in N$  of  $D$  with respect to  $D_0$  is defined as the difference

$$\begin{aligned} h_x(D, D_0) &= h_{D, D_0}(p + (1, 0)) - h_{D, D_0}(p), \\ h_y(D, D_0) &= h_{D, D_0}(p + (0, 1)) - h_{D, D_0}(p) \end{aligned}$$

of the height function, which does not depend on the choice of  $p \in M_{\mathbb{R}} \setminus (D \cup D_0)$ . The dependence of the height change on the choice of the reference matching is given by

$$h(D, D_1) = h(D, D_0) - h(D_1, D_0)$$

for any three perfect matchings  $D$ ,  $D_0$  and  $D_1$ . We will often suppress the dependence of the height difference on the reference matching and just write  $h(D) = h(D, D_0)$ .

- The *characteristic polynomial* of  $G$  is the Laurent polynomial in two variables defined by

$$Z(x, y) = \sum_{D : \text{a perfect matching}} x^{h_x(D)} y^{h_y(D)}.$$

- The *characteristic polygon* is the Newton polygon of the characteristic polynomial, i.e. the convex hull of

$$\{(h_x(D), h_y(D)) \in N \mid D \text{ is a perfect matching}\}.$$

As an example, consider the dimer model given in Figure 2.1. This dimer model has six perfect matchings  $D_1, \dots, D_6$  shown in Figures 2.2–2.7. The captions in these figures show the height changes with respect to  $D_4$ , and Figure 2.8 shows an example of a height function. The characteristic polygon is shown in Figure 2.9.

### 3 Description of the algorithm

An element  $m \in M$  is *primitive* if it cannot be written as  $km'$  where  $m' \in M$  and  $k$  is an integer greater than one. The set of primitive elements of  $M$  will be denoted by  $M_{\text{prim}}$ .

- An *oriented line* on  $T^\vee$  is a pair  $L = (\pi(\ell), m)$  of the image  $\pi(\ell)$  of a line  $\ell$  in  $M_{\mathbb{R}}$  by the natural projection  $\pi : M_{\mathbb{R}} \rightarrow T^\vee = M_{\mathbb{R}}/M$  and a primitive element  $m \in M_{\text{prim}}$  in the tangent space of  $\ell$ .
- The map  $(\pi(\ell), m) \mapsto m$  from the set of oriented lines to  $M_{\text{prim}}$  is denoted by  $p$ .
- The image  $p(L)$  is called the *slope* of  $L$ .
- The set of oriented lines on  $T^\vee$  can be identified with the product  $M_{\text{prim}} \times S^1$ , where  $M_{\text{prim}}$  parametrizes the slope and  $S^1$  parametrizes the position of  $\pi(\ell)$  in the direction perpendicular to the slope.
- An *oriented line arrangement* on  $T^\vee$  is a finite set of oriented lines on  $T^\vee$ .
- An oriented line arrangement on  $T^\vee$  is *simple* if no three lines intersect at one point.
- A *cell* of an oriented line arrangement is a connected component of the complement of the union of lines.
- An *edge* of a cell is a connected component of the intersection of the boundary of the cell and a line in the arrangement.

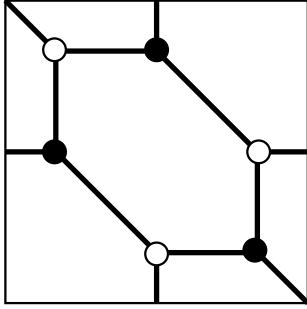


Figure 2.1: A dimer model

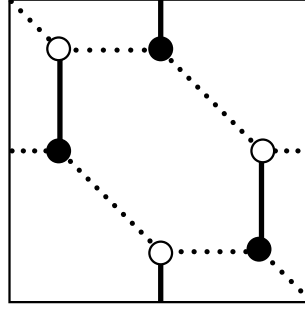


Figure 2.2:  $D_1 : (1, 0)$

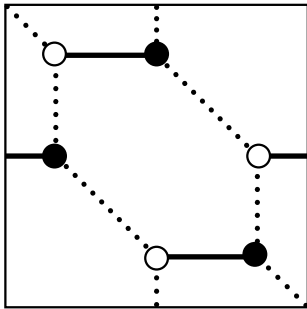


Figure 2.3:  $D_2 : (0, 1)$

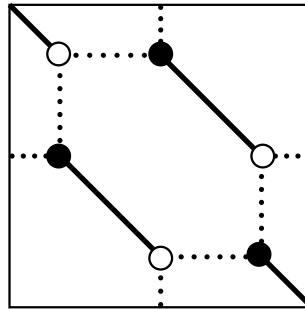


Figure 2.4:  $D_3 : (-1, -1)$

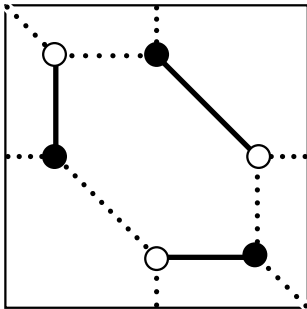


Figure 2.5:  $D_4 : (0, 0)$

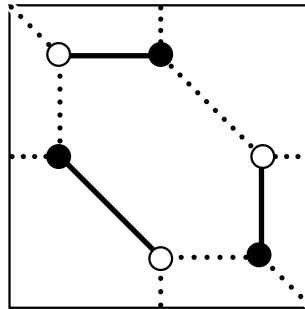


Figure 2.6:  $D_5 : (0, 0)$

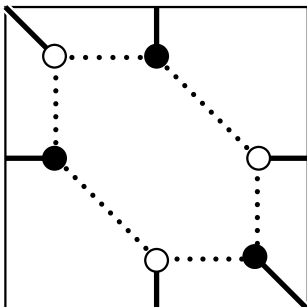


Figure 2.7:  $D_6 : (0, 0)$

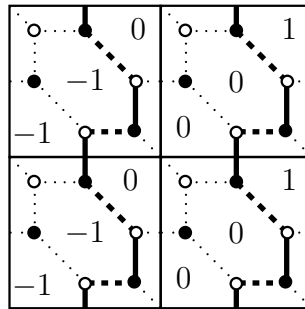


Figure 2.8: The height function for  $D_1$  with respect to  $D_4$

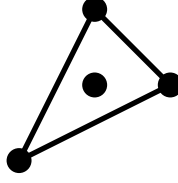


Figure 2.9: The characteristic polygon

- A *vertex* of a line arrangement is an intersection point of two lines.

The following concepts are at the heart of the algorithm of Hanany and Vegh:

- An edge of a cell of an oriented line arrangement has two orientations; one comes from the orientation of the line, and the other is the boundary orientation of the cell. A cell is said to be *white* if these two orientations agree for any of its edge, and *black* if they are opposite for any of its edge.
- A cell is *colored* if it is either black or white. Note that an edge in an oriented line arrangement bound two cells, and at most one of them can be colored.
- An oriented line arrangement is *admissible* if every edge bounds a colored cell.

Let  $\Delta \subset N_{\mathbb{R}}$  be a convex lattice polygon, i.e. the convex hull of a finite subset of  $N$ .

- An *edge* of  $\Delta$  is a connected component of  $\partial\Delta \setminus (\partial\Delta \cap N)$ . The set of edges of  $\Delta$  will be denoted by  $\mathcal{E}$ .
- The primitive outward normal vector to an edge  $e$  of  $\Delta$  is denoted by  $m(e) \in M_{\text{prim}}$ .
- The map  $\Delta \mapsto \{m(e)\}_{e \in \mathcal{E}}$  is a bijection from the set of convex lattice polygons up to translations to the set of finite collections of elements of  $M_{\text{prim}}$  summing up to zero.
- An oriented line arrangement  $\mathcal{A}$  is said to be *associated* with  $\Delta$  if  $\Delta$  corresponds to  $\{p(L)\}_{L \in \mathcal{A}}$  by the bijection above.

For example, the triangle  $\Delta_2$  shown in Figure 3.1 has four edges. There are two combinatorially distinct ways shown in Figure 3.2 and Figure 3.3 to arrange four lines in the directions of outward normal vectors of the edges of  $\Delta_2$ . In Figure 3.2, all edges bound colored polygons, whereas in Figure 3.3, the edges drawn in dotted lines do not bound any colored polygon. Hence the polygon  $\Delta_2$  in Figure 3.1 has a unique admissible arrangement.

Now we define the map  $\mathfrak{D}$  from the set of admissible arrangements to the set of dimer models:

**Definition 3.1.** Let  $\mathcal{A}$  be an admissible oriented line arrangement. Then the dimer model  $\mathfrak{D}(\mathcal{A}) = (B, W, E)$  associated with  $\mathcal{A}$  is defined as follows:

- The set  $W$  of white nodes is the set of the centers of gravities of white cells.

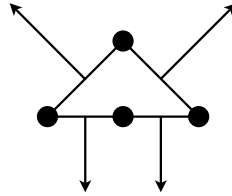


Figure 3.1: A triangle  $\Delta_2$

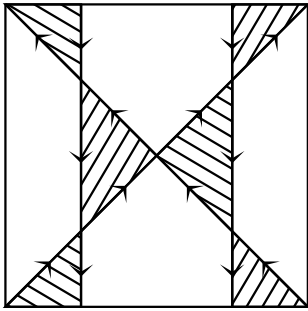


Figure 3.2: The admissible arrangement

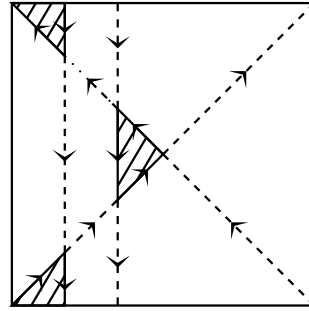


Figure 3.3: The non-admissible arrangement

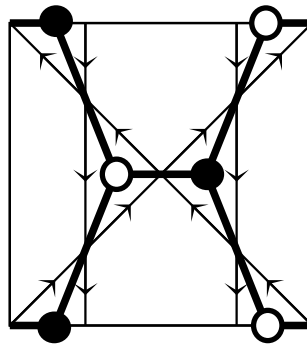


Figure 3.4: The dimer model

- The set  $B$  of black nodes is the set of the centers of gravities of black cells.
- Two nodes are connected by a straight line segment if the corresponding cells share a vertex.

As an example, Figure 3.4 shows the dimer model associated with the admissible arrangement in Figure 3.2.

Now we can formulate the linear Hanany-Vegh algorithm:

**Definition 3.2.** The *linear Hanany-Vegh algorithm* is defined as follows:

- Take a convex lattice polygon  $\Delta \subset N_{\mathbb{R}}$  as an input.
- The set  $\mathfrak{A}(\Delta)$  of oriented line arrangements  $\{L_a\}_a$  associated with  $\Delta$  is a real  $n$ -torus, where  $n$  is the number of edges of  $\Delta$ .
- The subset of  $\mathfrak{A}(\Delta)$  corresponding to simple arrangements will be denoted by  $\mathfrak{U}(\Delta)$ . The complement  $\mathfrak{A}(\Delta) \setminus \mathfrak{U}(\Delta)$  is a closed subset of real codimension one.
- Take a representative  $\mathfrak{V}(\Delta) \subset \mathfrak{U}(\Delta)$  of  $\pi_0(\mathfrak{U}(\Delta))$  and let  $\mathfrak{W}(\Delta) \subset \mathfrak{V}(\Delta)$  be the subset consisting of admissible arrangements.
- The output is the set  $\mathfrak{D}(\mathfrak{W}(\Delta))$  of dimer models associated with arrangements in  $\mathfrak{W}(\Delta)$ .

As an example, take the convex hull  $\Delta_4$  of

$$v_1 = (1, 0), \quad v_2 = (0, 1), \quad v_3 = (-1, 0), \quad \text{and} \quad v_4 = (-1, -1)$$

shown in Figure 3.5. The primitive outward normal vectors of the edges of  $\Delta_4$  are given by

$$m_1 = (1, 1), \quad m_2 = (-1, 1), \quad m_3 = (-1, 0), \quad \text{and} \quad m_4 = (1, -2).$$

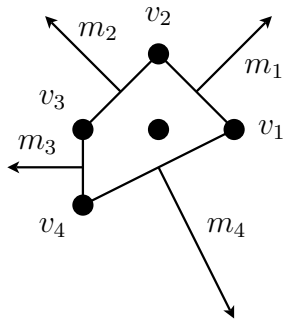


Figure 3.5: The lattice polygon  $\Delta_4$  with its primitive normal vectors

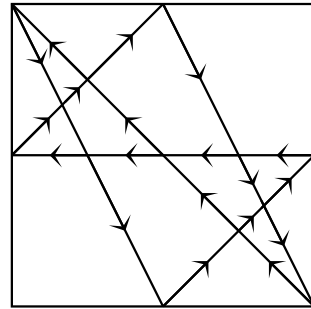


Figure 3.6: The unique admissible arrangement corresponding to  $\Delta_4$

**Lemma 3.3.** *There is a unique admissible oriented line arrangement associated with  $\Delta_4$ .*



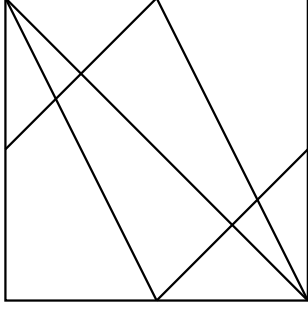


Figure 3.7: The unique arrangement of three lines in the directions of  $m_1$ ,  $m_2$  and  $m_4$

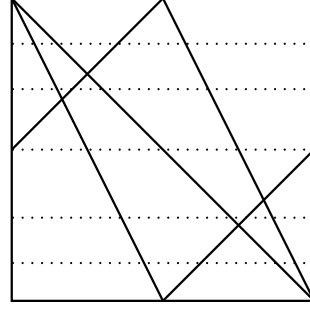


Figure 3.8: Five ways to insert the fourth line in the direction of  $m_3$

*Proof.* Figure 3.7 shows the unique arrangement of three oriented lines on the torus in the directions of  $m_1$ ,  $m_2$ , and  $m_4$ . There are five combinatorially distinct ways to insert a line into Figure 3.7 in the direction of  $m_3$  shown in Figure 3.8. In addition, since two of six intersection points of the three lines in Figure 3.7 are on the same horizontal level, there are two combinatorially distinct ways shown in Figure 3.9 and Figure 3.10 to perturb them a little and insert the fourth line. It is easy to see that out of these seven arrangements,

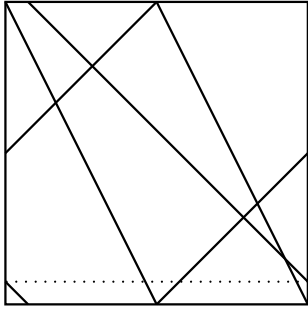


Figure 3.9: one way to perturb three lines to insert the fourth line

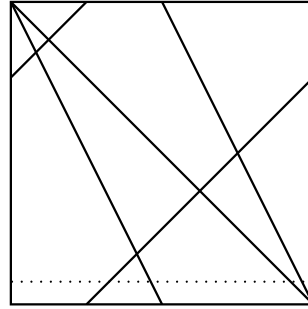


Figure 3.10: another way to perturb three lines to insert the fourth line

only the one shown in Figure 3.6 is admissible.  $\square$

Hence the output of the linear Hanany-Vegh algorithm consists of only one dimer model shown in Figure 3.11 in this case.

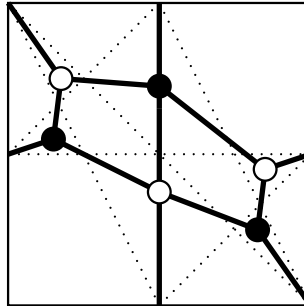


Figure 3.11: The dimer model

## 4 Zig-zag paths and isoradiality

The following notion is due to Duffin [6] and Mercat [26]:

**Definition 4.1.** A dimer model is *isoradial* if one can choose an embedding of the graph into the torus  $T^\vee$  so that every face of the graph is a polygon inscribed in a circle of a fixed radius with respect to a flat metric on  $T^\vee$ . Here, the circumcenter of any face must be contained in the face.

The following notion is introduced by Kenyon and Schlenker [22].

**Definition 4.2.** A *zig-zag path* is a path on a dimer model which makes a maximum turn to the right on a white node and maximum turn to the left on a black node.

If a dimer model comes from a lattice polygon through the linear Hanany-Vegh algorithm, then the set of zig-zag path can naturally be identified with the set of oriented lines in the admissible arrangement. Figure 4.1 shows an example of this identification.

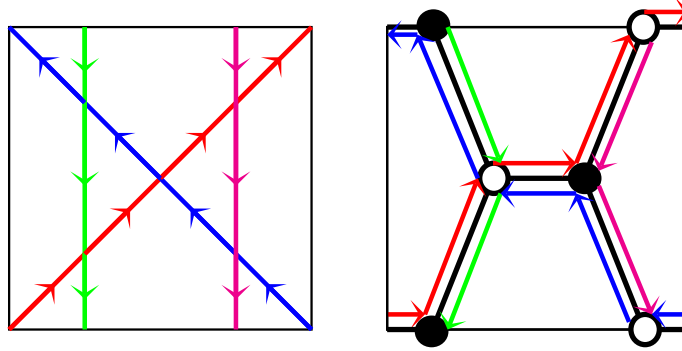


Figure 4.1: An admissible arrangement and zig-zag paths

A dimer model is isoradial if and only if zig-zag paths behave like straight lines:

**Theorem 4.3** (Kenyon and Schlenker [22, Theorem 5.1]). *A dimer model is isoradial if and only if the following conditions are satisfied:*

1. *Every zig-zag path is a simple closed curve.*
2. *The lift of any pair of zig-zag paths to the universal cover of the torus intersect at most once.*

Since zig-zag paths in a dimer model obtained through the linear Hanany-Vegh algorithm clearly satisfies these conditions, Theorem 4.3 immediately implies the following:

**Corollary 4.4.** *A dimer model obtained by the linear Hanany-Vegh algorithm is isoradial.*

The following notion is slightly weaker than isoradiality:

**Definition 4.5** ([16, Definition 5.2]). A dimer model is *consistent* if

- no zig-zag path has a self-intersection on the universal cover,
- no zig-zag path on the universal cover is a closed path, and

- no pair of zig-zag paths intersect each other on the universal cover in the same direction more than once.

One can formulate the *consistent Hanany-Vegh algorithm* by enlarging the domain of the brute-force search from the set of oriented line arrangements to the set of arrangements of oriented curves satisfying the three conditions in Definition 4.5. The orientations are given by the homology classes of the curves instead of the tangent spaces to the lines. Note that for a convex lattice polygon  $\Delta$ , the number of combinatorial types of arrangements of oriented curves associated with  $\Delta$  satisfying the conditions in Definition 4.5 is finite. One can also formulate the *isoradial Hanany-Vegh algorithm* by restricting to arrangements satisfying the conditions in Theorem 4.3.

The following theorem shows that Hanany-Vegh algorithms are inverse algorithms:

**Theorem 4.6** (Gulotta [13, Theorem 3.3], Ishii and Ueda [16, Corollary 8.3]). *If the set of zig-zag paths on a consistent dimer model  $G$  is associated with a lattice polygon  $\Delta$ , then the characteristic polygon of  $G$  coincides with  $\Delta$  up to translation.*

## 5 Dimer models and McKay quivers

We recall the description of the McKay quiver for an abelian subgroup of  $SL_3(\mathbb{C})$  as the dual of a hexagonal tiling on a torus [28, 31] and prove Theorem 1.2 in this section.

### 5.1 Quivers with potentials

A *quiver* consists of

- a set  $V$  of vertices,
- a set  $A$  of arrows, and
- two maps  $s, t : A \rightarrow V$  from  $A$  to  $V$ .

For an arrow  $a \in A$ , the vertices  $s(a)$  and  $t(a)$  are said to be the *source* and the *target* of  $a$  respectively. A *path* on a quiver is an ordered set of arrows  $(a_n, a_{n-1}, \dots, a_1)$  such that  $s(a_{i+1}) = t(a_i)$  for  $i = 1, \dots, n-1$ . We also allow for a path of length zero, starting and ending at the same vertex. The *path algebra*  $\mathbb{C}Q$  of a quiver  $Q = (V, A, s, t)$  is the algebra spanned by the set of paths as a vector space, and the multiplication is defined by the concatenation of paths;

$$(b_m, \dots, b_1) \cdot (a_n, \dots, a_1) = \begin{cases} (b_m, \dots, b_1, a_n, \dots, a_1) & s(b_1) = t(a_n), \\ 0 & \text{otherwise.} \end{cases}$$

A *quiver with relations* is a pair of a quiver and a two-sided ideal  $\mathcal{I}$  of its path algebra.

Let  $p = (a_n, \dots, a_1)$  be an oriented cycle on the quiver, i.e. the class of a path satisfying  $s(a_1) = t(a_n)$  up to a cyclic change of the starting point. For an arrow  $b$ , the *derivative* of  $p$  by  $b$  is defined by

$$\frac{\partial p}{\partial b} = \sum_{i=1}^n \delta_{a_i, b}(a_{i-1}, a_{i-2}, \dots, a_1, a_n, a_{n-1}, \dots, a_{i+1}),$$

where

$$\delta_{a,b} = \begin{cases} 1 & a = b, \\ 0 & \text{otherwise.} \end{cases}$$

This derivation extends to formal sums of oriented cycles by linearity.

A *potential* on a quiver is a formal sum  $\Phi$  of oriented cycles, which defines an ideal  $\mathcal{I} = (\partial\Phi)$  of relations generated by the derivatives  $\partial\Phi/\partial a$  for all the arrows  $a$  of the quiver;

$$(\partial\Phi) = \left( \frac{\partial\Phi}{\partial a} \right)_{a \in A}.$$

The most basic example is the quiver with  $V = \{v\}$  and  $A = \{x, y, z\}$ . Since there is only one vertex, the maps  $s$  and  $t$  must be constant. Consider the potential

$$\Phi = yxz - xyz.$$

The corresponding ideal is given by

$$\begin{aligned} (\partial\Phi) &= \left( \frac{\partial\Phi}{\partial x}, \frac{\partial\Phi}{\partial y}, \frac{\partial\Phi}{\partial z} \right) \\ &= (yz - zy, zx - xz, xy - yx). \end{aligned}$$

The resulting path algebra with relations is just the polynomial ring in three variables;

$$\mathbb{C}\langle x, y, z \rangle / (\partial\Phi) \cong \mathbb{C}[x, y, z].$$

See Ginzburg [12] and references therein for more on algebras associated with quivers with potentials.

## 5.2 McKay quivers

Let  $G$  be a finite subgroup of  $GL_n(\mathbb{C})$ . The *McKay quiver* of  $G$  is a quiver whose set of vertices is the set of irreducible representations of  $G$ , and the number  $a_{\sigma\tau}$  of arrows from  $\sigma$  to  $\tau$  is given by the multiplicity of  $\tau$  in the tensor product of  $\sigma$  with the dual representation  $\rho_{\text{Nat}}^\vee$  of the natural representation of  $G$ ;

$$\sigma \otimes \rho_{\text{Nat}}^\vee = \bigoplus_{\tau} \tau^{\otimes a_{\sigma\tau}}.$$

A path of length two from  $\sigma$  to  $\tau$  corresponds to an element of

$$\text{Hom}_G(\sigma \otimes \rho_{\text{Nat}}^\vee \otimes \rho_{\text{Nat}}^\vee, \tau).$$

The McKay quiver comes with relations generated by the kernel of the map

$$\sigma \otimes \rho_{\text{Nat}}^\vee \otimes \rho_{\text{Nat}}^\vee \rightarrow \sigma \otimes (\text{Sym}^2 \rho_{\text{Nat}}^\vee).$$

When  $G$  is an abelian subgroup  $A$  of  $SL_3(\mathbb{C})$ , the McKay quiver has the following description: Assume that  $A$  is contained in the diagonal subgroup, and let

$$\pi_i : A \rightarrow \mathbb{C}^\times, \quad i = 1, 2, 3,$$

be the projections to the  $i$ -th diagonal component, viewed as a one-dimensional representation of  $A$ . The set of vertices is the set  $\text{Irrep}(A)$  of irreducible representations of  $A$ , and for each vertex  $\rho \in \text{Irrep}(A)$ , there exist three arrows  $x_\rho$ ,  $y_\rho$ , and  $z_\rho$ , ending at the vertices  $\rho \otimes \pi_1^\vee$ ,  $\rho \otimes \pi_2^\vee$ , and  $\rho \otimes \pi_3^\vee$  respectively. The relations come from the potential

$$\Phi = xzy - xyz, \quad (5.1)$$

where  $x = \sum_\rho x_\rho$ ,  $y = \sum_\rho y_\rho$ , and  $z = \sum_\rho z_\rho$ .

### 5.3 Toric Calabi-Yau 3-folds associated with lattice polygons

Let  $\tilde{N} = N \oplus \mathbb{Z}$  be a free abelian group of rank three and  $\tilde{M} = M \oplus \mathbb{Z}$  be the dual group. For a lattice polygon  $\Delta \subset N_{\mathbb{R}}$ , let  $\sigma$  be the cone over  $\Delta \times \{1\} \subset \tilde{N}_{\mathbb{R}}$  and  $\Sigma$  be the fan in  $\tilde{N}_{\mathbb{R}}$  consisting of  $\sigma$  and its faces. Let  $\{\tilde{v}_i\}_{i=1}^r$  be the set of primitive generators of one-dimensional cones of  $\Sigma$ , and

$$\tilde{\phi} : \mathbb{Z}^r \rightarrow \tilde{N}$$

be the map which send the  $i$ -th standard coordinate vector  $e_i \in \mathbb{Z}^r$  to  $\tilde{v}_i \in \tilde{N}$ . Let

$$\tilde{\mathbb{T}} = \tilde{N} \otimes \mathbb{C}^\times = \text{Spec } \mathbb{C}[\tilde{M}]$$

be a three-dimensional torus. The group

$$K = \text{Ker}(\tilde{\phi} \otimes \mathbb{C}^\times : (\mathbb{C}^\times)^r \rightarrow \tilde{\mathbb{T}}) \subset (\mathbb{C}^\times)^r$$

naturally acts on  $\mathbb{C}^r$ , and the toric variety  $X$  associated with  $\Sigma$  is the quotient of  $\mathbb{C}^r$  by the action of  $K$ ;

$$X = \mathbb{C}^r / K.$$

The monoid ring

$$R = \mathbb{C}[\sigma^\vee]$$

of the dual cone

$$\sigma^\vee = \left\{ m \in \tilde{M} \mid \langle m, n \rangle \geq 0, \ n \in \sigma \right\} \subset \tilde{M}$$

is the coordinate ring of  $X$ ;

$$X = \text{Spec } R.$$

When  $\Delta$  is the convex hull of

$$v_1 = (p, q), \quad v_2 = (r, s), \quad v_3 = (0, 0),$$

then the map  $\tilde{\phi} : \mathbb{Z}^3 \rightarrow \tilde{N}$  is given by

$$(a, b, c) \mapsto (pa + rb, qa + rb, a + b + c),$$

so that the map  $\tilde{\phi} \otimes \mathbb{C}^\times : \mathbb{Z}^3 \rightarrow \tilde{\mathbb{T}}$  is given by

$$(\alpha, \beta, \gamma) \mapsto (\alpha^p \beta^r, \alpha^q \beta^s, \alpha \beta \gamma).$$

It follows that the toric variety associated with  $\Delta$  is the quotient

$$X = \mathbb{C}^3 / A$$

where

$$A = \left\{ (\alpha, \beta, \gamma) \in (\mathbb{C}^\times)^3 \mid \alpha^p \beta^r = \alpha^q \beta^s = \alpha \beta \gamma = 1 \right\}.$$

## 5.4 McKay quivers on the torus

The McKay quiver of an abelian subgroup of  $SL_3(\mathbb{C})$  can naturally be drawn on a real 2-torus as follows: Let  $N_1 = \mathbb{Z}^2$  be a free abelian group of rank two and  $M_1 = \text{Hom}(N_1, \mathbb{Z})$  be the dual group. Identify the torus

$$\mathbb{T}_1 = N_1 \otimes \mathbb{C}^\times = \text{Spec } \mathbb{C}[M_1]$$

with a maximal torus

$$\{\text{diag}(\alpha, \beta, \gamma) \in SL_3(\mathbb{C}) \mid \alpha\beta\gamma = 1\}$$

of  $SL_3(\mathbb{C})$ , so that the group

$$A = \{\text{diag}(\alpha, \beta, \gamma) \in SL_3(\mathbb{C}) \mid \alpha^p \beta^r = \alpha^q \beta^s = \alpha\beta\gamma = 1\}$$

is identified with the kernel of the map

$$\begin{array}{ccc} \phi \otimes \mathbb{C}^\times : & \mathbb{T}_1 & \rightarrow \mathbb{T} \\ & \Downarrow & \Downarrow \\ & (\alpha, \beta) & \mapsto (\alpha^p \beta^r, \alpha^q \beta^s), \end{array}$$

where  $\phi : N_1 \rightarrow N$  is the linear map given by the matrix

$$P = \begin{pmatrix} p & r \\ q & s \end{pmatrix}.$$

The short exact sequence

$$1 \rightarrow A \rightarrow \mathbb{T}_1 \xrightarrow{\phi \otimes \mathbb{C}^\times} \mathbb{T} \rightarrow 1$$

of abelian groups induces an exact sequence

$$0 \rightarrow M \xrightarrow{\psi} M_1 \rightarrow \text{Irrep}(A) \rightarrow 0$$

of characters, where  $\psi$  is the adjoint map of  $\phi : N_1 \rightarrow N$  represented by the transposed matrix of  $P$ .

Now consider the infinite quiver in Figure 5.1 drawn on  $M_1 \otimes \mathbb{R} \cong M_{\mathbb{R}}$ , whose set of vertices is  $M_1$  and whose set of arrows consists of  $x_{i,j}$ ,  $y_{i,j}$  and  $z_{i,j}$  for  $(i, j) \in M_1$  such that

$$s(x_{i,j}) = s(y_{i,j}) = s(z_{i,j}) = (i, j)$$

and

$$t(x_{i,j}) = (i+1, j), \quad t(y_{i,j}) = (i, j+1), \quad t(z_{i,j}) = (i-1, j-1).$$

The McKay quiver for  $A$  is the quotient of this quiver by the natural action of  $M$ .

As an example, consider the case when  $\Delta$  is the convex hull of  $(2, 1)$ ,  $(1, 3)$  and  $(0, 0)$  shown in Figure 5.2. The map  $\phi$  is presented by the matrix

$$P = \begin{pmatrix} 2 & 1 \\ 1 & 3 \end{pmatrix},$$

and the subgroup  $A$  is given by

$$A = \{(\alpha, \beta, \gamma) \in \mathbb{T}_1 \mid \alpha^2 \beta = \alpha \beta^3 = \alpha \beta \gamma = 1\},$$

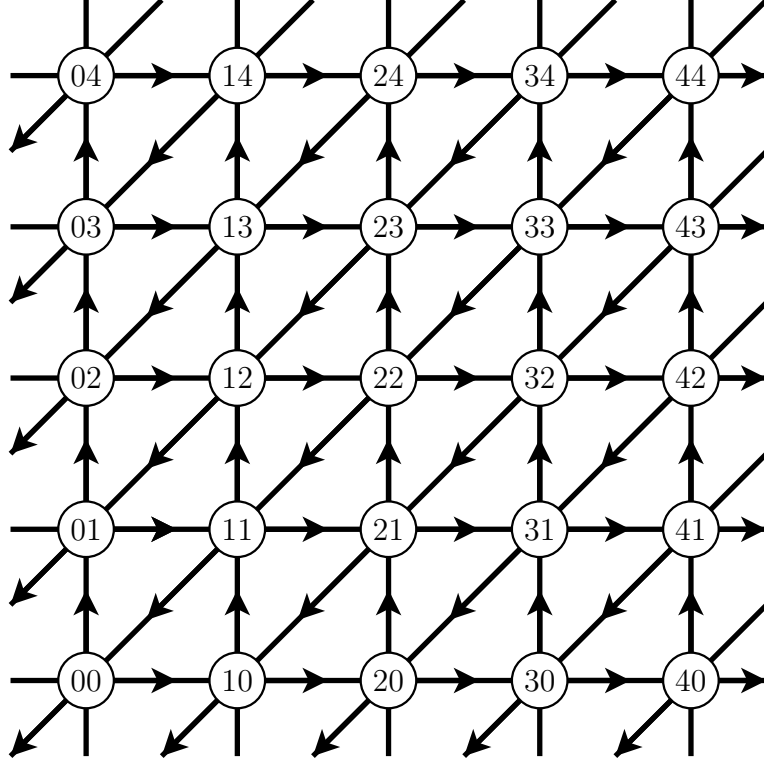


Figure 5.1: The periodic quiver

which is isomorphic to the image of

$$\begin{array}{ccc} \rho_{\text{Nat}} : \mathbb{Z}/5\mathbb{Z} & \rightarrow & \mathbb{T} \\ \cup & & \cup \\ [1] & \mapsto & (\zeta, \zeta^3, \zeta) \end{array}$$

where  $\zeta = \exp(2\pi\sqrt{-1}/5)$ . The quotient of the periodic quiver in Figure 5.1 by the action of  $M$  is shown in Figure 5.3, where fundamental regions of the action are shown in red.

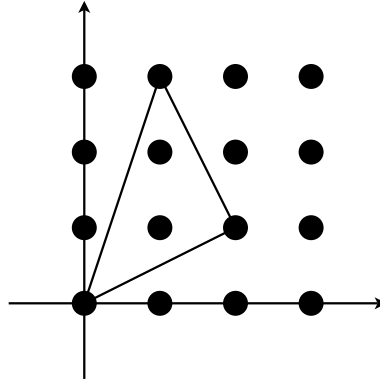


Figure 5.2: The triangle  $\Delta_5$

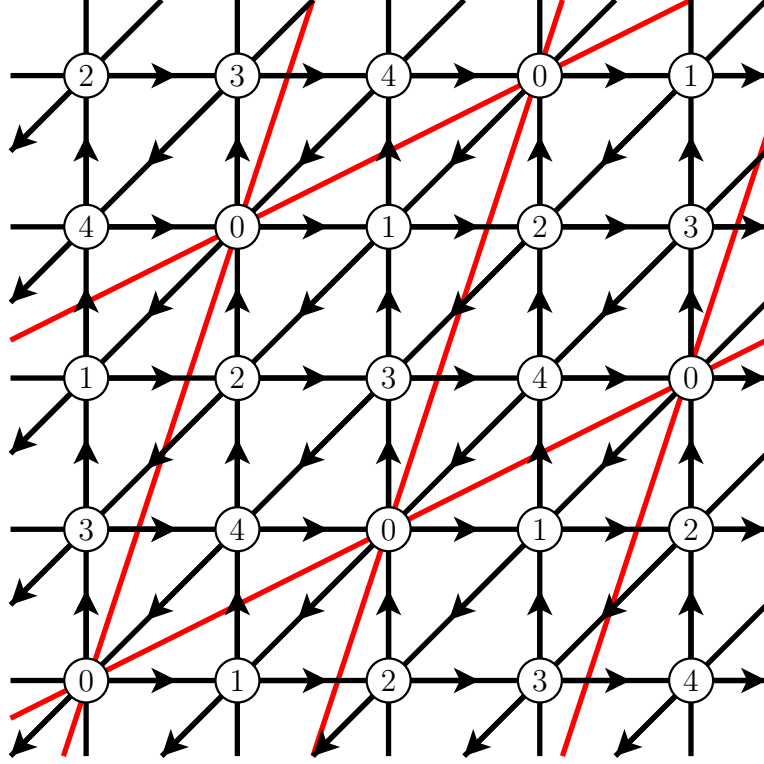


Figure 5.3: The McKay quiver

## 5.5 A quiver with potential from a dimer model

Note that the dual graph of the quiver in Figure 5.3 is a hexagonal tiling of the torus  $T^\vee = M_{\mathbb{R}}/M$  shown in Figure 5.4. The colors of the nodes of the dual graph is chosen so that a white node is always on the right of an arrow. Observe that the potential (5.1), which gives the relations of the McKay quiver, is the signed sum of cycles around the nodes of this graph;

$$\Phi = \sum_{w \in W} p_w - \sum_{b \in B} p_b. \quad (5.2)$$

This motivates the following definition of the quiver with potential associated with a dimer model  $G = (B, W, E)$ :

- The set  $V$  of vertices is the set of faces of  $G$ .
- The set  $A$  of arrows is the set  $E$  of edges of the graph. The directions of the arrows are determined by the colors of the vertices of the graph, so that the white vertex  $w \in W$  is on the right of the arrow.
- A node  $n \in B \amalg W$  determines an oriented cycle  $p_n$  of the quiver around it, and the potential is defined as the signed sum (5.2) over such cycles.

A hexagonal tiling of a torus can naturally be identified with the McKay quiver of an abelian subgroup of  $SL_3(\mathbb{C})$  in this way.



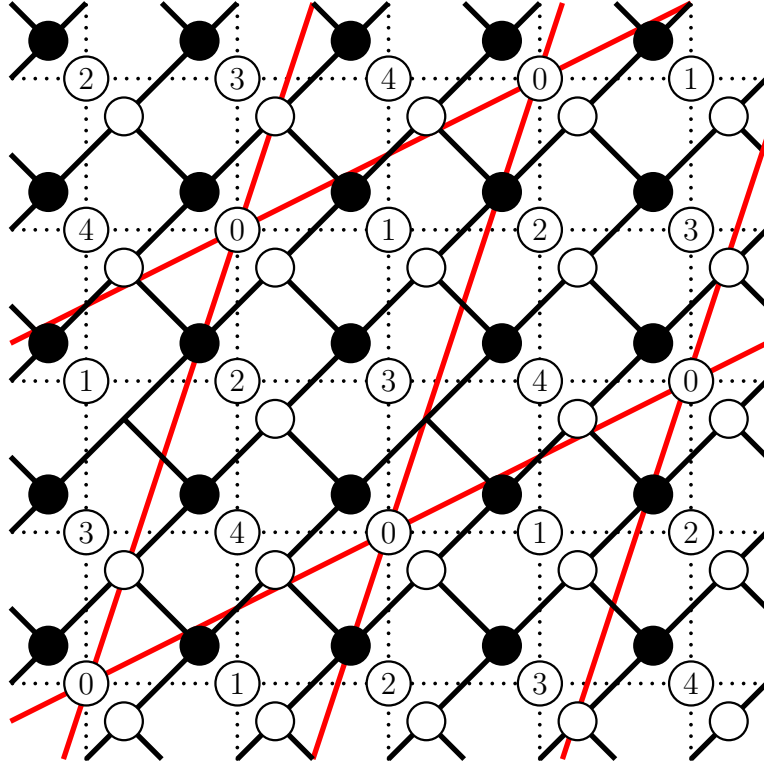


Figure 5.4: The dual honeycomb graph

## 5.6 The linear Hanany-Vegh algorithm on triangles

Now we prove Theorem 1.2. First note that given three slopes, there is only one way to form a polygon whose edges has one of these slopes and the boundary is positively oriented. This unique arrangement is the triangle shown in Figure 5.5, and an example of a polygon with unoriented boundary is shown in Figure 5.6.

For an arrangement of oriented lines to be admissible, each of the vertices of the triangle in Figure 5.5 must be contained in another triangle, whose boundary is negatively oriented. Again, there is a unique such arrangement, and Figure 5.7 shows two of these adjacent triangles.

By repeating the same argument, one obtains two new triangles in Figure 5.8, and then another triangle in Figure 5.9. It follows that the hexagonal tiling of the the torus which locally looks as in Figure 5.10 is the unique output of the linear Hanany-Vegh algorithm on a triangle  $\Delta$ . It is clear that this tiling is dual to the McKay quiver associated with  $\Delta$ , and Theorem 1.2 is proved.

## 6 Coamoebas and Newton polygons

For a Laurent polynomial

$$W(x, y) = \sum_{(i,j) \in N} a_{ij} x^i y^j$$

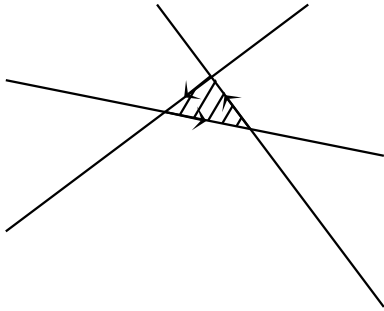


Figure 5.5: The unique positively-oriented polygon

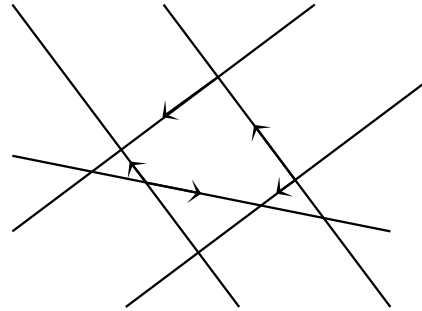


Figure 5.6: an example of an unoriented pentagon

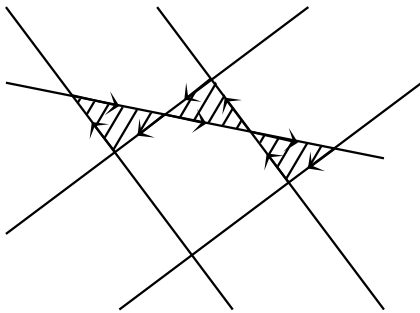


Figure 5.7: Two of the adjacent triangles

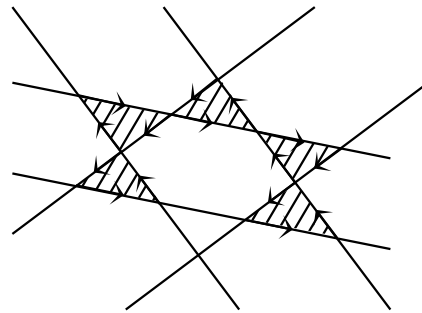


Figure 5.8: Two more triangles

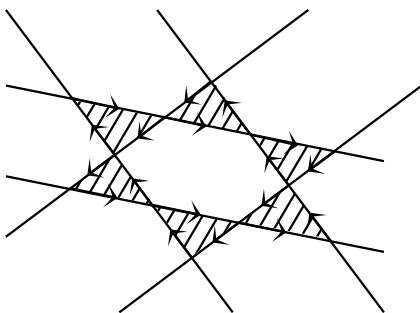


Figure 5.9: Yet another triangle

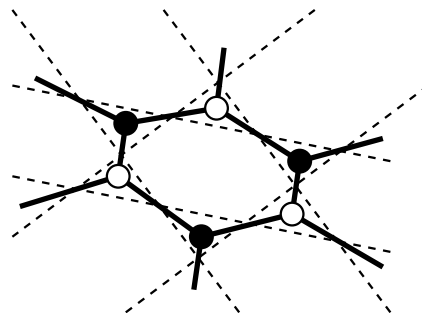


Figure 5.10: The hexagonal tiling

in two variables, its *Newton polygon* is defined as the convex hull of  $(i, j) \in N$  such that  $a_{ij} \neq 0$ ;

$$\Delta = \text{Conv}\{(i, j) \in N \mid a_{ij} \neq 0\} \subset N_{\mathbb{R}}.$$

It gives a regular map

$$W : \mathbb{T}^{\vee} \rightarrow \mathbb{C}$$

from the torus  $\mathbb{T}^{\vee} = M \otimes \mathbb{C}^{\times} = \text{Spec } \mathbb{C}[N]$  dual to  $\mathbb{T} = N \otimes \mathbb{C}^{\times}$ . The *coamoeba* of  $W^{-1}(0) \subset \mathbb{T}^{\vee}$  is its image under the argument map

$$\begin{aligned} \text{Arg} : \quad \mathbb{T}^{\vee} &\rightarrow T^{\vee} \\ \Psi &\quad \Psi \\ (x, y) &\mapsto \frac{1}{2\pi}(\arg x, \arg y). \end{aligned}$$

For an edge  $e$  of  $\Delta$ , let  $(n(e), m(e)) \in M$  be the primitive outward normal vector of  $e$  and  $l(e)$  be the integer such that the defining equation for the edge  $e$  is given by

$$n(e)i + m(e)j = l(e).$$

The *leading term* of  $W$  with respect to the edge  $e$  is defined by

$$W_e(x, y) = \sum_{n(e)i + m(e)j = l(e)} a_{ij} x^i y^j.$$

This is indeed the leading term if we put

$$(x, y) = (r^{n(e)}u, r^{m(e)}v), \quad r \in \mathbb{R} \text{ and } u, v \in \mathbb{C}^{\times}$$

and take the  $r \rightarrow \infty$  limit;

$$P(r^{n(e)}u, r^{m(e)}v) = r^{l(e)}W_e(u, v) + O(r^{l(e)-1}).$$

Now assume that for an edge  $e$ , the leading term  $W_e(x, y)$  is a binomial

$$W_e(x, y) = a_1 x^{i_1} y^{j_1} + a_2 x^{i_2} y^{j_2},$$

where  $a_1, a_2 \in \mathbb{C}$  and  $(i_1, j_1), (i_2, j_2) \in N$ . Put  $\alpha_i = \arg(a_i)$  for  $i = 1, 2$  and

$$(x, y) = (r^{n(e)}|a_2|e(\theta), r^{m(e)}|a_1|e(\phi)),$$

where  $e(x) = \exp(2\pi\sqrt{-1}x)$  for  $x \in \mathbb{R}/\mathbb{Z}$ . Then the leading behavior of  $W$  as  $r \rightarrow \infty$  is given by

$$r^{l(e)}W_e(e(\theta), e(\phi)) = r^{l(e)}|a_1 a_2| \{e(\alpha_1 + i_1\theta + j_1\phi) + e(\alpha_2 + i_2\theta + j_2\phi)\}. \quad (6.1)$$

Hence the coamoeba of  $W^{-1}(0)$  asymptotes in this limit to the line

$$(\alpha_2 - \alpha_1) + (i_2 - i_1)\theta + (j_2 - j_1)\phi + \frac{1}{2} = 0 \pmod{\mathbb{Z}}$$

on the torus  $T^{\vee}$ . This line will be called an *asymptotic boundary* of the coamoeba of  $W^{-1}(0)$ .

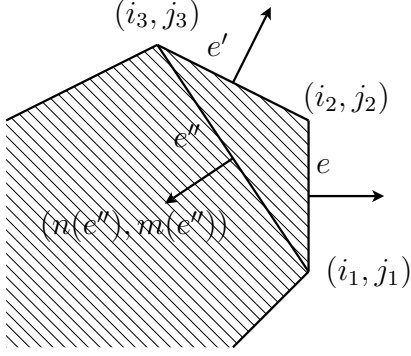


Figure 6.1: A pair of adjacent edges of the Newton polygon

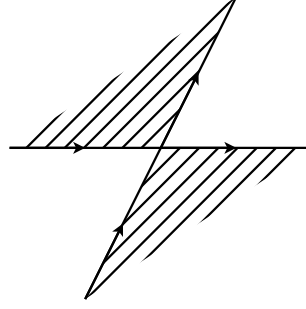


Figure 6.2: The leading behavior of the coamoeba near an intersection of asymptotic boundaries.

The asymptotic boundary has a natural orientation coming from the outward normal vector of the edge of  $\Delta$ . To understand the role of this orientation, take a pair of adjacent edges  $e$  and  $e'$  of  $\Delta$  as in Figure 6.1 and consider the behavior of the coamoeba of  $W^{-1}(0)$  near the intersection of asymptotic boundaries corresponding to  $e$  and  $e'$ . Assume that the leading terms corresponding to  $e$  and  $e'$  are binomials

$$\begin{aligned} W_e(x, y) &= \mathbf{e}(\alpha)x^{i_1}y^{j_1} + \mathbf{e}(\beta)x^{i_2}y^{j_2}, \\ W_{e'}(x, y) &= \mathbf{e}(\beta)x^{i_2}y^{j_2} + \mathbf{e}(\gamma)x^{i_3}y^{j_3} \end{aligned}$$

for some  $\alpha, \beta, \gamma \in \mathbb{R}/\mathbb{Z}$  and  $(i_1, j_1), (i_2, j_2), (i_3, j_3) \in N$ . Put

$$W_{ee'}(x, y) = \mathbf{e}(\alpha)x^{i_1}y^{j_1} + \mathbf{e}(\beta)x^{i_2}y^{j_2} + \mathbf{e}(\gamma)x^{i_3}y^{j_3}.$$

Assume further that all the coefficients of  $W$  corresponding to interior lattice points of the Newton polygon of  $W_{ee'}$  vanish. Then  $W_{ee'}$  is the sum of the leading term and the sub-leading term of  $W$  as one puts

$$(x, y) = (r^{-n(e'')}u, r^{-m(e'')}v), \quad r \in \mathbb{R}^{>0} \text{ and } u, v \in \mathbb{C}^\times,$$

and take the  $r \rightarrow \infty$  limit. Here,  $(n(e''), m(e'')) \in M$  is the primitive outward normal vector of the edge  $e''$  of the Newton polygon of  $W_{ee'}$  shown in Figure 6.1. The coamoeba for the sum of three monomials will be analyzed in Section 7; the asymptotic boundaries coincide with the actual boundaries of the coamoeba, and the orientations on the asymptotic boundaries determine which side of the boundary belongs to the coamoeba. Hence the orientations of asymptotic boundaries determine the leading behavior of the coamoeba near the intersections of asymptotic boundaries as in Figure 6.2.

## 7 Coamoebas for triangles

We discuss the coamoeba of  $W^{-1}(0) \subset \mathbb{T}^\vee$  in this section, where  $W$  is the sum of three Laurent monomials. The strategy is to reduce to the simplest case  $W(x, y) = 1 + x + y$  by a finite cover of the torus.

**Theorem 7.1.** *Let  $\Delta$  be a lattice triangle and  $W$  be the Laurent polynomial obtained as the sum of monomials corresponding to the vertices of  $\Delta$ . Then the coamoeba of  $W^{-1}(0)$  has the following description:*

- The set  $\mathcal{A}$  of asymptotic boundaries, equipped with the orientation coming from the outward normal vectors of  $\Delta$ , is an admissible arrangement of oriented lines.
- The coamoeba is the union of colored cells and vertices of  $\mathcal{A}$ .
- The restriction of the argument map to the inverse image of a colored cell is a diffeomorphism. It is orientation-preserving if the cell is white, and reversing if the cell is black.
- The inverse image of a vertex of  $\mathcal{A}$  by the argument map is homeomorphic to an open interval.

*Proof.* We first consider the simplest case

$$W_1(x, y) = 1 + x + y \in \mathbb{C}[N_1]$$

where  $N_1 \cong \mathbb{Z}^2$  is a free abelian group of rank two. It gives a regular map

$$\mathbb{T}_1^\vee = M_1 \otimes \mathbb{C}^\times \rightarrow \mathbb{C}$$

where  $M_1 = \text{Hom}(N_1, \mathbb{Z})$  is the dual group of  $N_1$ , and the coamoeba of  $W_1^{-1}(0)$  is a subset of  $T_1^\vee = M_1 \otimes \mathbb{R}/M_1$ . The zero locus of  $W_1$  is obtained by gluing two disks

$$D_1 = \{(x, y) \in (\mathbb{C}^\times)^2 \mid \Im(x) > 0, y = -1 - x\}$$

and

$$D_2 = \{(x, y) \in (\mathbb{C}^\times)^2 \mid \Im(x) < 0, y = -1 - x\}$$

along three intervals

$$I_1 = \{(x, y) \in (\mathbb{R})^2 \mid x < -1, y = -1 - x\},$$

$$I_2 = \{(x, y) \in (\mathbb{R})^2 \mid -1 < x < 0, y = -1 - x\},$$

and

$$I_3 = \{(x, y) \in (\mathbb{R})^2 \mid x > 0, y = -1 - x\}.$$

Define

$$U_1 = \{(\theta, \phi) \in T_1^\vee \mid 0 < \theta < \frac{1}{2}, -\frac{1}{2} < \phi < -\frac{1}{2} + \theta\}$$

and

$$U_2 = \{(\theta, \phi) \in T_1^\vee \mid -\frac{1}{2} < \theta < 0, \frac{1}{2} + \theta < \phi < \frac{1}{2}\}$$

as in Figure 7.1. Then the argument map gives an orientation-reversing homeomorphism from  $D_1$  to  $U_1$  and an orientation-preserving homeomorphism from  $D_2$  to  $U_2$ , and maps  $I_1$ ,  $I_2$ , and  $I_3$  to  $(\frac{1}{2}, 0)$ ,  $(\frac{1}{2}, \frac{1}{2})$ , and  $(0, \frac{1}{2})$  respectively.

Now we discuss the general case. Assume that  $W$  is given by

$$W(x, y) = 1 + x^p y^q + x^r y^s \in \mathbb{C}[N]$$

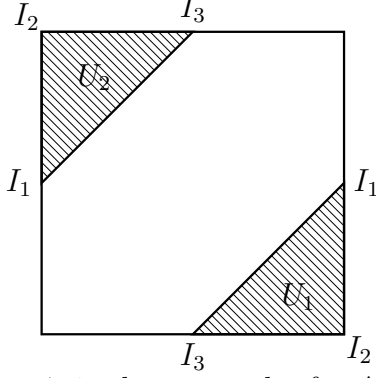


Figure 7.1: the coamoeba for  $\Delta_1$

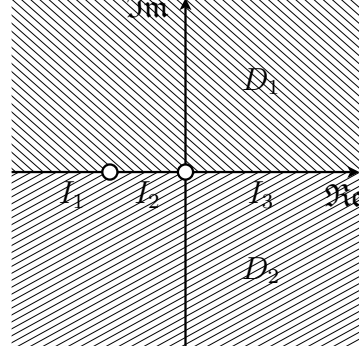


Figure 7.2: the glued surface

for some integers  $p, q, r$  and  $s$ . Note that one has a commutative diagram

$$\begin{array}{ccc} \mathbb{T}^\vee & \xrightarrow{\psi \otimes \mathbb{C}^\times} & \mathbb{T}_1^\vee \\ & \searrow W & \downarrow W_1 \\ & & \mathbb{C} \end{array}$$

where  $\psi : M \rightarrow M_1$  is the linear map represented by the matrix  $\begin{pmatrix} p & q \\ r & s \end{pmatrix}$ . It follows from the commutative diagram

$$\begin{array}{ccc} \mathbb{T}^\vee & \xrightarrow{\psi \otimes \mathbb{C}^\times} & \mathbb{T}_1^\vee \\ \text{Arg} \downarrow & & \downarrow \text{Arg} \\ T^\vee & \xrightarrow{\psi \otimes (\mathbb{R}/\mathbb{Z})} & T_1^\vee \end{array}$$

that the coamoeba of  $W^{-1}(0)$  is the pull-back by  $\psi \otimes (\mathbb{R}/\mathbb{Z})$  of the coamoeba of  $W_1^{-1}(0)$ ;

$$\text{Arg}(W^{-1}(0)) = (\psi \otimes (\mathbb{R}/\mathbb{Z}))^{-1}(\text{Arg}(W_1^{-1}(0))).$$

This reduces the general case to the the case of  $W_1$  discussed above, and Theorem 7.1 is proved.  $\square$

**Acknowledgment:** We thank Kenji Fukaya for organizing a workshop in Kinosaki in March 2006 where this joint project has been initiated. K. U. thanks Alastair Craw for introducing him to the work of Hanany and Vegh, and providing helpful explanations and valuable comments. He also thanks Akira Ishii for collaborations which improved his understanding of dimer models. M. Y. thanks Tohru Eguchi and Akishi Kato for helpful comments. K. U. is supported by Grant-in-Aid for Young Scientists (No.18840029).

## References

- [1] Sergio Benvenuti, Leopoldo A. Pando Zayas, and Yuji Tachikawa. Triangle anomalies from Einstein manifolds. *Adv. Theor. Math. Phys.*, 10(3):395–432, 2006.
- [2] Nathan Broomhead. Dimer models and Calabi-Yau algebras. arXiv:0901.4662.

- [3] Agostino Butti and Alberto Zaffaroni.  $R$ -charges from toric diagrams and the equivalence of  $a$ -maximization and  $Z$ -minimization. *J. High Energy Phys.*, (11):019, 42 pp. (electronic), 2005.
- [4] Agostino Butti and Alberto Zaffaroni. From toric geometry to quiver gauge theory: the equivalence of  $a$ -maximization and  $Z$ -minimization. *Fortschr. Phys.*, 54(5-6):309–316, 2006.
- [5] Ben Davison. Consistency conditions for brane tilings. arXiv:0812.4185.
- [6] R. J. Duffin. Potential theory on a rhombic lattice. *J. Combinatorial Theory*, 5:258–272, 1968.
- [7] Bo Feng, Yang-Hui He, Kristian D. Kennaway, and Cumrun Vafa. Dimer models from mirror symmetry and quivering amoebae. *Adv. Theor. Math. Phys.*, 12(3):489–545, 2008.
- [8] R. H. Fowler and G. S. Rushbrooke. An attempt to extend the statistical theory of perfect solutions. *Trans. Faraday Soc.*, 33:1272 – 1294, 1937.
- [9] Sebastián Franco, Amihay Hanany, Dario Martelli, James Sparks, David Vegh, and Brian Wecht. Gauge theories from toric geometry and brane tilings. *J. High Energy Phys.*, (1):128, 40 pp. (electronic), 2006.
- [10] Sebastián Franco, Amihay Hanany, David Vegh, Brian Wecht, and Kristian D. Kennaway. Brane dimers and quiver gauge theories. *J. High Energy Phys.*, (1):096, 48 pp. (electronic), 2006.
- [11] Sebastián Franco and David Vegh. Moduli spaces of gauge theories from dimer models: proof of the correspondence. *J. High Energy Phys.*, (11):054, 26 pp. (electronic), 2006.
- [12] Victor Ginzburg. Calabi-Yau algebras. math.AG/0612139, 2006.
- [13] Daniel R. Gulotta. Properly ordered dimers,  $R$ -charges, and an efficient inverse algorithm. *J. High Energy Phys.*, (10):014, 31, 2008.
- [14] Amihay Hanany and Kristian D. Kennaway. Dimer models and toric diagrams. hep-th/0503149, 2005.
- [15] Amihay Hanany and David Vegh. Quivers, tilings, branes and rhombi. *J. High Energy Phys.*, (10):029, 35, 2007.
- [16] Akira Ishii and Kazushi Ueda. Dimer models and the special McKay correspondence. arXiv:0905.0059.
- [17] Akira Ishii and Kazushi Ueda. On moduli spaces of quiver representations associated with dimer models. In *Higher dimensional algebraic varieties and vector bundles*, RIMS Kôkyûroku Bessatsu, B9, pages 127–141. Res. Inst. Math. Sci. (RIMS), Kyoto, 2008.

- [18] P. W. Kasteleyn. Dimer statistics and phase transitions. *J. Mathematical Phys.*, 4:287–293, 1963.
- [19] Akishi Kato. Zonotopes and four-dimensional superconformal field theories. *J. High Energy Phys.*, (6):037, 30 pp. (electronic), 2007.
- [20] Richard Kenyon. An introduction to the dimer model. In *School and Conference on Probability Theory*, ICTP Lect. Notes, XVII, pages 267–304 (electronic). Abdus Salam Int. Cent. Theoret. Phys., Trieste, 2004.
- [21] Richard Kenyon, Andrei Okounkov, and Scott Sheffield. Dimers and amoebae. *Ann. of Math. (2)*, 163(3):1019–1056, 2006.
- [22] Richard Kenyon and Jean-Marc Schlenker. Rhombic embeddings of planar quad-graphs. *Trans. Amer. Math. Soc.*, 357(9):3443–3458 (electronic), 2005.
- [23] Sangmin Lee and Soo-Jong Rey. Comments on anomalies and charges of toric-quiver duals. *J. High Energy Phys.*, (3):068, 21 pp. (electronic), 2006.
- [24] Dario Martelli, James Sparks, and Shing-Tung Yau. The geometric dual of  $a$ -maximisation for toric Sasaki-Einstein manifolds. *Comm. Math. Phys.*, 268(1):39–65, 2006.
- [25] Dario Martelli, James Sparks, and Shing-Tung Yau. Sasaki-Einstein manifolds and volume minimisation. *Comm. Math. Phys.*, 280(3):611–673, 2008.
- [26] Christian Mercat. Discrete Riemann surfaces and the Ising model. *Comm. Math. Phys.*, 218(1):177–216, 2001.
- [27] Sergey Mozgovoy and Markus Reineke. On the noncommutative Donaldson-Thomas invariants arising from brane tilings. arXiv:0809.0117.
- [28] Iku Nakamura. Hilbert schemes of abelian group orbits. *J. Algebraic Geom.*, 10(4):757–779, 2001.
- [29] Andrei Okounkov, Nikolai Reshetikhin, and Cumrun Vafa. Quantum Calabi-Yau and classical crystals. In *The unity of mathematics*, volume 244 of *Progr. Math.*, pages 597–618. Birkhäuser Boston, Boston, MA, 2006.
- [30] Hiroshi Ooguri and Masahito Yamazaki. Emergent Calabi-Yau geometry. *Phys. Rev. Lett.*, 102(16):161601, 4, 2009.
- [31] Miles Reid. McKay correspondence. alg-geom/9702016.
- [32] Jan Stienstra. Computation of principal A-determinants through dimer dynamics. arXiv:0901.3681.
- [33] Jan Stienstra. Hypergeometric systems in two variables, quivers, dimers and dessins d’enfants. In *Modular forms and string duality*, volume 54 of *Fields Inst. Commun.*, pages 125–161. Amer. Math. Soc., Providence, RI, 2008.



- [34] Kazushi Ueda and Masahito Yamazaki. Homological mirror symmetry for toric orbifolds of toric del Pezzo surfaces. [math.AG/0703267](#).

Kazushi Ueda

Department of Mathematics, Graduate School of Science, Osaka University, Machikaneyama 1-1, Toyonaka, Osaka, 560-0043, Japan.

*e-mail address* : [kazushi@math.sci.osaka-u.ac.jp](mailto:kazushi@math.sci.osaka-u.ac.jp)

Masahito Yamazaki

Department of Physics, Graduate School of Science, University of Tokyo, Hongo 7-3-1, Bunkyo-ku, Tokyo, 113-0033, Japan

*e-mail address* : [yamazaki@hep-th.phys.s.u-tokyo.ac.jp](mailto:yamazaki@hep-th.phys.s.u-tokyo.ac.jp)